

Restricting Voltage Deviation of DC Microgrids with Critical and Ordinary Nodes [★]

Handong Bai ^a, Peng Li ^b, Hongwei Zhang ^{b*}

^a*School of Electrical Engineering, Yellow River Conservancy Technical Institute, Kaifeng, Henan 475004, P.R. China*

^b*School of Mechanical Engineering and Automation, Harbin Institute of Technology, Shenzhen, Guangdong 518055, P.R. China*

Abstract

Restricting bus voltage deviation is crucial for normal operation of multi-bus DC microgrids, yet it has received insufficient attention due to the conflict between two main control objectives in DC microgrids, i.e., voltage regulation and current sharing. By revealing a necessary and sufficient condition for achieving these two objectives, this paper proposes a compromised distributed control algorithm, which regulates the voltage deviation of all buses by relaxing the accuracy of current sharing. Moreover, for a class of DC Microgrids consisting of both critical nodes and ordinary nodes, this paper proposes a distributed control algorithm that restricts the voltage deviation of critical nodes and simultaneously keeps the current sharing of ordinary nodes. This algorithm also works under plug-and-play settings. Simulations illustrate our theory.

Key words: compromised control; current sharing; DC microgrid; Kron reduction; voltage deviation.

1 Introduction

Replacing traditional fossil energy sources with renewable ones is fundamental for sustainable development of energy systems (Lund, 2007). Yet this transition on the generation side leads to significant changes in both the structure and dynamics of power systems. One important difference is that, in contrast to conventional generators, most renewable generators (such as photovoltaic units and fuel cells), and storage units (such as batteries and ultra-capacitors), have direct current (DC) characteristics (Elsayed et al., 2015; Justo et al., 2013). Furthermore, they are often connected at low or medium voltage levels and termed distributed generators (DGs) (Elsayed et al., 2015).

As an effective and reliable integration of DGs, DC

microgrids have been attracting increasing attention in both power and control communities in recent years (Che and Shahidehpour, 2014; De Persis et al., 2018; Dragičević et al., 2015; Liu et al., 2023; Nahata et al., 2020; Zhao and Dörfler, 2015). In DC microgrids, two common control objectives are current sharing and voltage regulation (Dragičević et al., 2015). The former addresses the problem of sharing the total load current among DGs in proportion to their current ratings. The latter aims to regulate each bus voltage to the rated value of the system. However, there exists a conflict between current sharing and voltage regulation since current sharing depends on voltage deviations between neighboring buses (Bai et al., 2022; Han et al., 2019). Consequently, most existing control methods prioritize current sharing over voltage regulation, and often achieve voltage balancing instead that fixes the steady-state average or weighted-average voltage over all buses at a rated value (Cucuzzella et al., 2018; Nahata et al., 2022; Nasirian et al., 2015; Shafiee et al., 2014; Trip et al., 2019; Tucci et al., 2018). But these works do not consider bus voltage deviation from the rated value, and tend to destabilize the voltage balance during the plug-and-play of DGs.

For normal operation of loads, voltage deviations of buses from the rated value should be kept within a reasonable range depending on the requirements of

* This work was supported in part by Shenzhen Science and Technology Program under Grant GXWD20231129102406001 and Grant JCYJ20220818102416036, and in part by the Key Scientific Research Projects of Higher Education Institutions in Henan Province under Grant 24A120011.

* Corresponding author.

Email addresses: baihandong@yrcti.edu.cn (Handong Bai), lipeng2020@hit.edu.cn (Peng Li), hwzhang@hit.edu.cn (Hongwei Zhang).

loads. In general, admissible maximum voltage deviation (AMVD) is set to about 5% of the rated voltage (Nasirian et al., 2015; Prabhakaran et al., 2018). Even though accurate current sharing and voltage balancing are achieved, some loads may work abnormally or even be damaged when some voltage deviations exceed AMVD. To avoid this situation, bus voltage deviations should be strictly restricted within AMVD, especially for those voltage-sensitive loads.

The issue of voltage deviation restriction was concerned in Han et al. (2019), and a compromised control method was proposed to achieve a trade-off between current sharing and voltage regulation. However, the bounds for voltage deviation are not analyzed, and the relation between voltage deviation and current sharing is not clear. Ding et al. (2018) proposed a distributed optimal control strategy to achieve a compromised objective between accurate current sharing and voltage regulation. But the quantitative relationship between control parameters and voltage deviations is missing, making the algorithm less practical. In Cucuzzella et al. (2018), a manifold was designed to take both current sharing and voltage regulation into consideration, in which voltage deviation can be regulated. Yet, the mechanism of interaction between current sharing and voltage regulation is not disclosed, and thus it is hard to adjust the accuracies of current sharing and voltage regulation for certain requirements of the microgrids. Voltage deviation regulation was further investigated in our recent work (Bai et al., 2022), where a distributed compromised control method was proposed, and an existence condition and the design guidance for the trade-off parameter are given. Using this proposed method, continuous regulation from accurate current sharing to reference voltage consensus can be achieved, but all bus voltages cannot be regulated to the rated value simultaneously. Thus this method fails in scenarios when strict voltage deviation is required. To the best of our knowledge, a distributed control scheme that enables continuous regulation from accurate current sharing to bus voltage consensus with detailed analysis of steady-state characteristics has not been reported in literature.

It is also worth noting that, in distributed control of DC microgrids, most existing control methods treat all nodes equally. However, this is not the case in practical situations, where different kinds of DGs will play different roles. For example, photovoltaics are used to supply power as much as possible, while batteries are responsible for supporting voltage to stabilize the operation of DC microgrids. On the other hand, different kinds of loads tolerate different voltage deviations. For example, data centers are voltage-sensitive loads that often require a very strict voltage deviation of less than 2% of the rated voltage (Pratt et al., 2007), while voltage-insensitive loads like residential facilities can even tolerate an AMVD of 8% of the rated voltage. Therefore, in DC microgrids, nodes should be classified from the

control point of view. Unfortunately, most existing voltage regulation strategies treat all nodes equally. Suppose control parameters are adjusted to reduce voltage deviations of some voltage-sensitive buses. In that case, voltage deviations of other voltage-insensitive buses will also be reduced, resulting in unnecessary deterioration of current sharing for both voltage sensitive and insensitive nodes in DC microgrids (Bai et al., 2022; Ding et al., 2018; Han et al., 2019). However, considering the relationship between current sharing and voltage regulation, the deterioration of the current sharing of voltage-insensitive nodes might be avoided by relaxing the voltage deviation requirement. Moreover, in some scenarios, only a few bus voltage deviations are greater than their AMVD, while most other buses are operated within their normal ranges. In these cases, a reasonable objective is to reduce only those excessive voltage deviations while maintaining current sharing of those nodes with admissible voltage deviations. To the best of our knowledge, such control issues have not been investigated so far.

Moreover, most existing voltage balancing control methods, including average voltage regulation (De Persis et al., 2018; Nasirian et al., 2015; Tucci et al., 2018) and weighted-average voltage regulation (Cucuzzella et al., 2018; Nahata et al., 2022; Trip et al., 2019), cannot deal with the issue of average voltage fluctuation under plug-and-play situations. In Nasirian et al. (2015), a distributed observer is used to estimate the average voltage over all buses in a DC microgrid, and then the observed average voltage is regulated to the rated value. However, since this algorithm is not robust to initialization error (Kia et al., 2019), when any DG is plugged in or out of the microgrid, the average voltage cannot be observed correctly. A robust dynamic average consensus algorithm to initialization error is proposed in Kia et al. (2019), where the average voltage can be observed correctly under DG plugging or unplugging situations, but a transient voltage fluctuation may happen for all buses, including some voltage-sensitive buses. Weighted-average voltage regulation methods in Nahata et al. (2022) and Trip et al. (2019) suffer from the same issue of bus voltage fluctuation. For DC microgrids consisting of both voltage sensitive nodes and insensitive nodes, it is desirable to restrict the voltage deviation for voltage-sensitive buses under plug-and-play of voltage-insensitive nodes. Unfortunately, this problem is still open. One technical challenge lies in that the communication network of the DC microgrid treats all nodes equally without differentiating sensitive nodes from insensitive ones.

Motivated by the aforementioned statements, this paper aims to design distributed control laws for the DC microgrids with both critical and ordinary nodes, such that a trade-off between current sharing and voltage regulation can be achieved, and the voltage deviation and voltage balancing of critical nodes can be regulated without sacrificing the accuracy of current sharing among the ordi-

nary nodes¹. The main contributions of this paper are as follows.

- (a) Control objectives of accurate current sharing, accurate voltage consensus and voltage-current compromise are uniformly characterised by indices of voltage and current deviation ratios, which facilitates the controller design. In addition, a necessary and sufficient condition for the existence of conflict between accurate current sharing and voltage consensus is given.
- (b) A distributed cooperative control strategy is proposed to achieve continuous regulation from accurate current sharing to bus voltage consensus. The monotonicity of voltage and current deviation ratios is guaranteed, which is of practical significance for the design of the trade-off factor.
- (c) Kron reduction is applied to reduce the topology of the communication network, which is the key to separate critical nodes from ordinary nodes.
- (d) A distributed control scheme is proposed, and voltage deviation restriction of critical nodes and accurate current sharing of ordinary nodes are achieved simultaneously. Moreover, this algorithm works in DG plugging and unplugging situations. Compared with existing methods that treat all nodes equally, the scenarios studied in this paper are more practical.

The rest of this paper is organized as follows. Preliminaries on graph theory, DC microgrid modeling and the conflict of voltage regulation and current sharing are given in Section 2. In Section 3, a voltage-current compromised control problem is formulated and corresponding control law is proposed; and a rigorous steady state analysis of the closed-loop system is provided. In Section 4, a distributed control scheme considering voltage balancing and compromised control for critical nodes as well as accurate current sharing for ordinary nodes is proposed. The performances of the proposed control laws are illustrated by simulation examples in Section 5. Section 6 concludes this paper.

2 Preliminary

2.1 Notation

The notation used throughout this paper is rather standard. Let \mathbb{R}^n , $\mathbb{R}_{\geq 0}^n$ and $\mathbb{R}_{\leq 0}^n$ be the n -dimensional real,

¹ To facilitate the development, in this paper, we classify all nodes into critical nodes and ordinary ones. The former include voltage-sensitive nodes, points of common coupling and energy storage nodes, which requires strict voltage deviations. The latter comprising voltage-insensitive nodes and renewable generation nodes pursues accurate current sharing and usually work under relaxed voltage deviations.

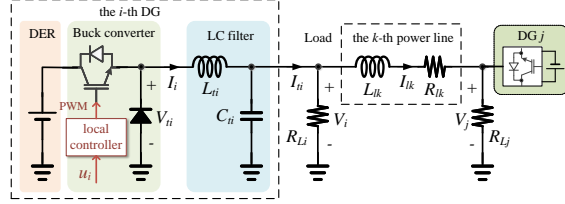


Fig. 1. Electrical scheme of the i -th DG

nonnegative and non-positive real vector space, respectively. The identity matrix (of appropriate dimension) is denoted by \mathbf{E} . The notation $\mathbf{0}$ denotes zero vector or matrix with appropriate dimensions. Let $\mathbf{1}_n = [1, \dots, 1]^T \in \mathbb{R}^n$. A diagonal matrix is denoted as $\text{diag}(g_1, g_2, \dots, g_n)$ with g_i being the i -th diagonal entry. A matrix $\mathbf{A} = [a_{ij}] \in \mathbb{R}^{n \times n}$ is said to be nonnegative (positive), denoted by $\mathbf{A} \geq \mathbf{0}$ ($\mathbf{A} > \mathbf{0}$), if $a_{ij} \geq 0$ ($a_{ij} > 0$), $\forall i, j$. Matrix $|\mathbf{A}|$ is obtained by taking element-wise absolute value of the matrix \mathbf{A} .

2.2 Graph theory

The communication network of a DC microgrid is modeled as a graph $\mathcal{G} = (\mathcal{V}, \mathcal{E})$, where $\mathcal{V} = \{v_1, \dots, v_N\}$ denotes the set of nodes, i.e., DGs or buses, and $\mathcal{E} \subseteq \mathcal{V} \times \mathcal{V}$ denotes the set of edges, i.e., communication links. The topology of a graph \mathcal{G} is captured by its adjacency matrix $\mathcal{A} = [a_{ij}] \in \mathbb{R}^{N \times N}$, where a_{ij} is the weight of edge (v_j, v_i) , and $a_{ij} > 0$ if $(v_j, v_i) \in \mathcal{E}$; otherwise $a_{ij} = 0$. When $a_{ij} = a_{ji}$, $\forall i, j$, the graph is undirected; otherwise, it is directed. A graph with adjacency matrix \mathcal{A} is denoted as $\mathcal{G}(\mathcal{A})$. The Laplacian matrix $\mathcal{L} = [l_{ij}] \in \mathbb{R}^{N \times N}$ of \mathcal{G} is defined as $l_{ii} = \sum_{j=1}^N a_{ij}$ and $l_{ij} = -a_{ij}$ if $i \neq j$. A path from node v_i to v_j is a sequence of consecutive edges $\{(v_i, v_l), (v_l, v_m), \dots, (v_n, v_j)\}$. An undirected graph is connected, if there is a path between any two nodes. The adjacency matrix and Laplacian matrix of a connected undirected graph are irreducible (Lewis et al., 2014).

2.3 DC microgrid model

Considering a generic DC microgrid consisting of N ($N > 1$) nodes, whose electrical network has been reduced by Kron reduction (Dörfler and Bullo, 2013). A general electrical scheme of the i -th DG is shown in Fig. 1 (Trip et al., 2019), where V_{t_i} denotes the output voltage of the Buck converter of the i -th DG, L_{t_i} and C_{t_i} denote the inductance and capacitance of the LC filter respectively. Following standard practices (Cucuzzella et al., 2018; Nahata et al., 2020; Schiffer et al., 2016; Trip et al., 2019), we have

$$V_{t_i} = u_i, \quad (1)$$

where V_{t_i} is the output voltage of the i -th DG converter, and u_i is the associated control signal for this converter. Let $\mathbf{V}_t = [V_{t_1}, \dots, V_{t_N}]^T$ and $\mathbf{u} = [u_1, \dots, u_N]^T$.

Load modeling is not unified to characterize all different kinds of loads in a microgrid (Kundur, 1994). This paper considers loads of constant impedances with admittances as $\mathbf{Y}_L = \text{diag}(Y_{L_1}, \dots, Y_{L_N})$, with $Y_{L_i} = \frac{1}{R_{L_i}}, \forall i \in \{1, \dots, N\}$, where Y_{L_i}, R_{L_i} are conductance and resistance of the i -th load, respectively. Our results may be inaccurate for other type of load models, such as constant power loads (Liu et al., 2018).

Assume M power lines are connected to N buses in a DC microgrid. The dynamics of power lines can be modeled as (Kundur, 1994)

$$\mathbf{L}_l \dot{\mathbf{I}}_l = \mathbf{B}^T \mathbf{V} - \mathbf{R}_l \mathbf{I}_l, \quad (2)$$

where $\mathbf{V} = [V_1, \dots, V_N]^T \in \mathbb{R}^N$ and $\mathbf{I}_l = [I_{l_1}, \dots, I_{l_M}]^T \in \mathbb{R}^M$ denote bus voltages and the currents of power lines, respectively; $\mathbf{L}_l = \text{diag}(L_{l_1}, \dots, L_{l_M})$ and $\mathbf{R}_l = \text{diag}(R_{l_1}, \dots, R_{l_M}) \in \mathbb{R}_{\geq 0}^{M \times M}$ denote inductances and resistances of the power lines, respectively; $\mathbf{B} = [B_{ik}] \in \mathbb{R}^{N \times M}$ denotes the incidence matrix of electrical topology of the DC microgrid, in which $B_{ik} = +1$ (or $B_{ik} = -1$) if the i -th bus is the source (or the sink) of the k -th power line; otherwise, $B_{ik} = 0$. According to Kirchhoff's voltage and current laws, the dynamics of the output LC filters of the converters can be expressed as

$$\mathbf{L}_t \dot{\mathbf{I}} = \mathbf{V}_t - \mathbf{V} \quad (3a)$$

$$\mathbf{C}_t \dot{\mathbf{V}} = \mathbf{I} - \mathbf{Y}_L \mathbf{V} - \mathbf{B} \mathbf{I}_l, \quad (3b)$$

where $\mathbf{I} = [I_1, \dots, I_N]^T \in \mathbb{R}^N$ denotes the output currents of the DG converters; $\mathbf{L}_t = \text{diag}(L_{t_1}, \dots, L_{t_N})$ and $\mathbf{C}_t = \text{diag}(C_{t_1}, \dots, C_{t_N}) \in \mathbb{R}_{\geq 0}^{N \times N}$ denote inductances and capacitances of the LC filters, respectively.

2.4 Conflict of voltage consensus and current sharing

It is well known that, in DC microgrids, there exists a conflict between voltage regulation and current sharing (Bai et al., 2022; Han et al., 2019; Liu et al., 2023). In other words, proportional current sharing among DGs and maintaining the rated values for all bus voltages cannot be achieved simultaneously. This conflict will be rigorously analyzed in the sequel. The following definitions and fact are instrumental in this paper.

Definition 1 (Bai et al., 2022) *In a DC microgrid, the voltage deviation ratio (VDR) and the current deviation ratio (CDR) for the i -th DG are defined respectively as*

$$\Delta_i^V = \frac{V_i - V_{rat}}{V_{rat}} \quad \text{and} \quad \Delta_i^I = \frac{I_i^{pu} - I_{avg}^{pu}}{I_{avg}^{pu}},$$

where V_{rat} is the rated bus voltage of the DC microgrid, $I_i^{pu} = I_i/I_i^*$ is the output per-unit current of the DG

at node i with $I_i^* > 0$ being the current capacity of the i -th DG, and $I_{avg}^{pu} = \sum_{i=1}^N I_i^{pu}/N$. Furthermore, define the maximum voltage deviation ratio (MVDR) and the maximum current deviation ratio (MCDR) of the DC microgrid as $\Delta_{max}^V = \|\Delta^V\|_\infty$ and $\Delta_{max}^I = \|\Delta^I\|_\infty$, respectively, where $\Delta^V = [\Delta_1^V, \dots, \Delta_N^V]^T$, $\Delta^I = [\Delta_1^I, \dots, \Delta_N^I]^T$.

Based on the above notions, accurate current sharing and voltage consensus are further defined.

Definition 2 (Accurate current sharing) *In a DC microgrid, accurate current sharing among DGs is achieved if $\Delta_{max}^I = 0$, i.e., $\frac{I_i}{I_i^*} = \dots = \frac{I_N}{I_N^*} = I_{avg}^{pu}$.*

Definition 3 (Accurate voltage consensus) *In a DC microgrid, accurate voltage consensus among buses is achieved if $\Delta_{max}^V = 0$, i.e., $V_i = \dots = V_N = V_{rat}$.*

According to Def. 1, Def. 2 and Def. 3, it is straightforward to show that lower accuracy of current sharing (voltage consensus) corresponds to greater values of Δ_{max}^I (Δ_{max}^V).

Here arises a question whether voltage consensus and accurate current sharing can be achieved simultaneously. The following Fact answers this question. Before proposing the Fact, we need to establish a preliminary result.

Lemma 1 *Consider a DC microgrid described by (1), (2) and (3). The following identity holds:*

$$(\mathbf{Y} + \mathbf{Y}_L)^{-1} \mathbf{Y}_L \mathbf{1}_N = \mathbf{1}_N. \quad (4)$$

Proof: See Appendix A. \square

Fact 1 *Consider a DC microgrid described by (1), (2) and (3). In steady state, accurate current sharing and bus voltage consensus can be achieved simultaneously if and only if $\mathbf{Y}_L \mathbf{1}_N > 0$ and*

$$\frac{I_1^*}{Y_{L_1}} = \frac{I_2^*}{Y_{L_2}} = \dots = \frac{I_N^*}{Y_{L_N}}. \quad (5)$$

Proof: For given DC microgrid modeled by (1), (2) and (3), letting $\dot{\mathbf{I}}_l$, $\dot{\mathbf{I}}$ and $\dot{\mathbf{V}}$ equal to zero yields the steady state model of DC microgrids as follows.

$$\mathbf{V}_t - \mathbf{V} = 0 \quad (6a)$$

$$\mathbf{I} - \mathbf{Y}_L \mathbf{V} - \mathbf{Y} \mathbf{V} = 0, \quad (6b)$$

where $\mathbf{Y} = \mathbf{B} \mathbf{R}_l \mathbf{B}^T$ denotes the admittance matrix of the DC microgrid. Substituting $\mathbf{V} = V_{rat} \mathbf{1}_N + \Delta \mathbf{V}$ in (6b) gives $\mathbf{I} = (\mathbf{Y} + \mathbf{Y}_L)(V_{rat} \mathbf{1}_N + \Delta \mathbf{V})$. Moreover, since

$\mathbf{Y} + \mathbf{Y}_L$ is invertible (Bai et al., 2022), using $\Delta^V = \Delta \mathbf{V} / V_{rat}$ and Lemma 1, we have

$$\Delta^V = (\mathbf{Y} + \mathbf{Y}_L)^{-1} \left(\frac{\mathbf{I}}{V_{rat}} - \mathbf{Y}_L \mathbf{1}_N \right). \quad (7)$$

Since $(\mathbf{Y} + \mathbf{Y}_L)^{-1} > \mathbb{0}$ (Bai et al., 2022), it implies that $\Delta^V = \mathbb{0}$ as $\mathbf{I} = V_{rat} \mathbf{Y}_L \mathbf{1}_N$. Moreover, when accurate current sharing among DGs is attained, i.e., $\Delta_{max}^I = 0$, we have $\mathbf{I} = \alpha \mathbf{I}^*$ with α being a positive constant. Thus $\Delta^V = \mathbb{0}$ and $\Delta^I = \mathbb{0}$ if and only if $\mathbf{I}^* = \frac{V_{rat}}{\alpha} \mathbf{Y}_L \mathbf{1}_N$. \square

Remark 1 *It has been recognized that accurate current sharing always conflicts with voltage consensus (Bai et al., 2022; Han et al., 2019). However, Fact 1 discloses, for the first time, this conflict happens if only if condition (5) does not hold.*

Since condition (5) does not hold for general cases, the concept of the voltage-current compromise is required.

Definition 4 (Voltage-current compromise) *For a DC microgrid, let Δ^V denote the Δ_{max}^V for the case of accurate current sharing; and $\bar{\Delta}^I$ denote the Δ_{max}^I for the case of accurate voltage consensus. Then a voltage-current compromise is established if $\Delta_C^V < \bar{\Delta}^V$ and $\Delta_C^I < \bar{\Delta}^I$, where Δ_C^V and Δ_C^I are the Δ_{max}^V and Δ_{max}^I for the case of the voltage-current compromise, respectively.*

3 Voltage-current compromised control

3.1 Problem formulation

Fact 1 implies that, for given DGs and loads in a DC microgrid, if (5) does not hold, voltage deviations among DC buses can only be restricted by sacrificing the accuracy of current sharing. Therefore, the first problem considered in this paper can be formulated as follows.

Problem 1 *Consider a DC microgrid described by (1), (2) and (3).*

- Design a compromised control structure to achieve voltage-current compromise, where Δ_{max}^I and Δ_{max}^V are adjustable by control parameters.*
- Given an admissible maximum voltage deviation ratio Γ_V , choose appropriate control parameters to restrict voltage deviation subjecting to $\Delta_{max}^V \leq \Gamma_V$.*

According to Fact 1, it can be seen that if the i -th bus does not connect to a load directly, i.e., $Y_{L_i} = 0$, the bus voltage V_i cannot be regulated to a consensus value among the network. To address Problem 1, this circumstance is not considered in this section, and it is reasonable to make the following Assumption.

Assumption 1 *There is a load for each bus, i.e., $Y_{L_i} \neq 0, \forall i \in \{1, \dots, N\}$.*

The case where Assumption 1 does not hold will be addressed in Section 4.

3.2 Compromised control law design

So far, a consensus-based distributed secondary control law has been broadly used for accurate current sharing (Cucuzzella et al., 2018; Nahata et al., 2022; Nasirian et al., 2015; Tucci et al., 2018) with a generic form:

$$\dot{x}_i = \sum_{j=1}^N a_{ij} \left(\frac{I_j}{I_j^*} - \frac{I_i}{I_i^*} \right), \quad (8)$$

where $a_{ij} \geq 0$ are the elements of the adjacency matrix \mathcal{A} of the communication graph $\mathcal{G}(\mathcal{A})$, and $x_i, i \in \{1, \dots, N\}$ are state variables denoting different notions in different works, such as voltage correction terms (Nasirian et al., 2015), additional state variables (Cucuzzella et al., 2018; Nahata et al., 2022) and voltage deviations between voltage references and node voltages (Tucci et al., 2018). In steady state, accurate current sharing is achieved, i.e., $\frac{I_1}{I_1^*} = \frac{I_2}{I_2^*} = \dots = \frac{I_N}{I_N^*}$. However, the voltage deviation of each node from the rated value is not considered in the aforementioned works, which may lead to abnormal operation of the loads.

By modifying accurate current sharing control law (8) to regulate the voltage deviations of nodes and achieve voltage-current compromise of a DC microgrid, this paper proposes a compromised control law as

$$\dot{x}_i = \sum_{j=1}^N a_{ij} \left(\frac{I_j}{I_{r_j}} - \frac{I_i}{I_{r_i}} \right) \quad (9a)$$

$$I_{r_i} = \theta I_i^* + (1 - \theta) I_{b_i}, \quad (9b)$$

where $I_{b_i} = V_{rat} Y_{L_i}$, and $\theta \in [0, 1]$ is a trade-off factor indicating the degree of the compromise, which will be clarified in Corollary 1.

Remark 2 *Interestingly, by substituting controller (9) into a specific accurate current sharing control scheme, such as the ones in Cucuzzella et al. (2018); Nahata et al. (2022); Nasirian et al. (2015); Tucci et al. (2018), these works can be directly extended to solve the voltage-current compromised control problems.*

To illustrate the effectiveness of the proposed control method, we will apply controller (9) to the control scheme in Nasirian et al. (2015) to establish a compromised control scheme (see Fig. 2 for the control block

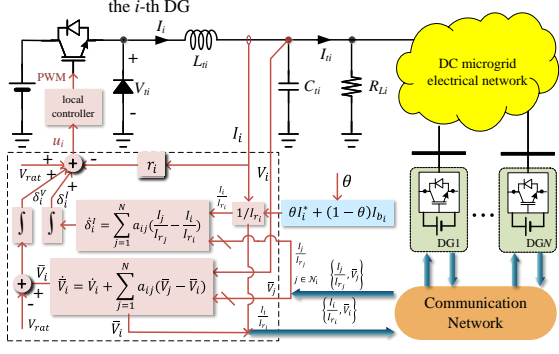


Fig. 2. Control block diagram of the DC microgrid with respect to controller (10) and (9)

diagram) as

$$u_i = V_{rat} - r_i I_i + \delta_i^I + \delta_i^V \quad (10a)$$

$$\delta_i^V = V_{rat} - \bar{V}_i \quad (10b)$$

$$\dot{\bar{V}}_i = \dot{V}_i + \sum_{j=1}^N a_{ij} (\bar{V}_j - \bar{V}_i) \quad (10c)$$

$$\delta_i^I = \sum_{j=1}^N a_{ij} \left(\frac{I_j}{I_{r_j}} - \frac{I_i}{I_{r_i}} \right) \quad (10d)$$

$$I_{r_i} = \theta I_i^* + (1 - \theta) I_{b_i}, \quad (10e)$$

where u_i is the reference signal of the local controller, r_i is the droop coefficient, δ_i^I and δ_i^V denote correction terms with respect to voltage and current, and \bar{V}_i is the estimation of node i with respect to the average voltage among all buses. Moreover, (10a) represents a droop control, (10b) is a voltage regulator to maintain average voltage among all buses to the rated value and (10c) is distributed average voltage observer. To achieve the control objectives in Problem 1, the communication graph $\mathcal{G}(\mathcal{A})$ is assumed to be undirected and connected (Nasirian et al., 2015). Note that the stability analysis of the closed-loop system under control scheme (10) is similar as that in Nasirian et al. (2015), and thus is omitted herein.

3.3 Steady state analysis

We are now about to analyze the steady state feature of the proposed method.

Theorem 1 Consider the DC microgrid (2) and (3) governed by (10). Suppose Assumption 1 hold. Then the steady state of the closed-loop system satisfies the following properties:

(a) For any given θ , the load current is shared among all DGs in the following proportion rule

$$\frac{I_1}{I_{r_1}} = \dots = \frac{I_N}{I_{r_N}} = \frac{1}{\mu\theta + 1 - \theta} > 0,$$

where $\mu = \frac{1}{NV_{rat}} \mathbf{1}_N^T (\mathbf{Y} + \mathbf{Y}_L)^{-1} \mathbf{I}^*$.

(b) The function $|\Delta^V(\theta)|$ is monotonically increasing on $\theta \in [0, 1]$, and

$$\Delta^V(\theta) = \frac{\theta}{(\mu - 1)\theta + 1} \Psi, \quad (11)$$

where $\Psi = \frac{1}{V_{rat}} (\mathbf{Y} + \mathbf{Y}_L)^{-1} \mathbf{I}^* - \mu \mathbf{1}_N$. Particularly, for $\theta \in [0, 1]$, we have

$$\begin{cases} \min_{\theta} |\Delta^V(\theta)| = \Delta^V(0) = 0 \\ \max_{\theta} |\Delta^V(\theta)| = |\Delta^V(1)| = \frac{1}{\mu} |\Psi|. \end{cases} \quad (12)$$

(c) The function $|\Delta^I(\theta)|$ is monotonically decreasing on $\theta \in [0, 1]$, and

$$\Delta^I(\theta) = \frac{1 - \theta}{\theta(1/\bar{I}_b^{pu} - 1) + 1} \Delta_b^I,$$

where $\bar{I}_b^{pu} = \frac{1}{N} \mathbf{1}_N^T \mathbf{I}_b^{pu}$ and $\Delta_b^I = (\mathbf{I}_b^{pu} - \bar{I}_b^{pu} \mathbf{1}_N) / \bar{I}_b^{pu}$ with $\mathbf{I}_b^{pu} = \text{diag}(\mathbf{I}^*)^{-1} \mathbf{I}_b$. Particularly, for $\theta \in [0, 1]$, we have

$$\begin{cases} \min_{\theta} |\Delta^I(\theta)| = \Delta^I(1) = 0 \\ \max_{\theta} |\Delta^I(\theta)| = |\Delta^I(0)| = |\Delta_b^I|. \end{cases} \quad (13)$$

Proof: Part (a).

Applying the similar analysis as in Nasirian et al. (2015), under controller (10), in the steady state, it is straightforward to show $\frac{I_1}{I_{r_1}} = \dots = \frac{I_N}{I_{r_N}} = \alpha$, where $\alpha > 0$ is a constant. Letting $\mathbf{I}_r = [I_{r_1}, \dots, I_{r_N}]^T$ and substituting $\mathbf{I} = \alpha \mathbf{I}_r$ into (7) yields

$$\Delta^V(\theta) = \frac{\alpha\theta}{V_{rat}} (\mathbf{Y} + \mathbf{Y}_L)^{-1} (\mathbf{I}^* - \mathbf{I}_b) - (1 - \alpha) \mathbf{1}_N. \quad (14)$$

Following similar system analysis as in Nasirian et al. (2015), we can show that voltage balancing is achieved, which further implies that $\mathbf{1}_N^T \Delta^V(\theta) = 0$. Hence, left multiplying (14) by $\mathbf{1}_N^T$ and substituting $\mathbf{I}_b = V_{rat} \mathbf{Y}_L \mathbf{1}_N$ into (14) yields

$$0 = \frac{\alpha\theta}{V_{rat}} \mathbf{1}_N^T (\mathbf{Y} + \mathbf{Y}_L)^{-1} (\mathbf{I}^* - V_{rat} \mathbf{Y}_L \mathbf{1}_N) - (1 - \alpha) N. \quad (15)$$

Then, let $\mu = \frac{1}{NV_{rat}} \mathbf{1}_N^T (\mathbf{Y} + \mathbf{Y}_L)^{-1} \mathbf{I}^*$ to further simplify (15) as

$$\alpha = \frac{1}{\mu\theta + 1 - \theta}. \quad (16)$$

Since $\mathbf{Y} + \mathbf{Y}_L$ is a nonsingular \mathcal{M} -matrix (Bai et al., 2022), and $\mathbf{I}^* > 0$, we have $\mu > 0$. Recalling $\theta \in [0, 1]$,

we have $\alpha > 0$.

Part (b).

Substituting (16) into (14) leads to

$$\begin{aligned}\Delta^V(\theta) &= \frac{\theta(\mathbf{Y} + \mathbf{Y}_L)^{-1} \mathbf{I}^*}{V_{rat}(\mu\theta + 1 - \theta)} - \frac{\mu\theta}{\mu\theta + 1 - \theta} \mathbf{1}_N \\ &= \frac{\theta}{\mu\theta + 1 - \theta} \Psi,\end{aligned}$$

where $\Psi = \frac{1}{V_{rat}}(\mathbf{Y} + \mathbf{Y}_L)^{-1} \mathbf{I}^* - \mu \mathbf{1}_N$. Therefore, since $\alpha > 0$ in (16) and $\theta \in [0, 1]$, we have $\frac{\theta}{\mu\theta + 1 - \theta} \geq 0$. Thus $|\Delta^V(\theta)|$ is monotonically increasing on $\theta \in [0, 1]$. Further, it is straightforward to obtain (12).

Part (c).

In the steady state, the output current $\mathbf{I} = \alpha \mathbf{I}_r = \alpha(\theta \mathbf{I}^* + (1 - \theta) \mathbf{I}_b)$. Therefore, we have

$$\mathbf{I}^{pu} = \alpha(\theta \mathbf{1}_N + (1 - \theta) \mathbf{I}_b^{pu}),$$

where $\mathbf{I}_b^{pu} = \text{diag}(\mathbf{I}^*)^{-1} \mathbf{I}_b$. By Definition 1, we have $\mathbf{I}^{pu} = \mathbf{I}_{avg}^{pu}(\Delta^I + \mathbf{1}_N)$ with $\mathbf{1}_N^T \Delta^I = 0$. Consequently,

$$\mathbf{I}_{avg}^{pu}(\Delta^I + \mathbf{1}_N) = \alpha(\theta \mathbf{1}_N + (1 - \theta) \mathbf{I}_b^{pu}), \quad (17)$$

which further implies, by left multiplying (17) by $\mathbf{1}_N^T$, that

$$\mathbf{I}_{avg}^{pu} = \alpha(\theta(1 - \bar{I}_b^{pu}) + \bar{I}_b^{pu}), \quad (18)$$

where $\bar{I}_b^{pu} = \frac{1}{N} \mathbf{1}_N^T \mathbf{I}_b^{pu}$. Hence, substituting (18) into (17) yields

$$\begin{aligned}\Delta^I(\theta) &= \frac{1 - \theta}{\theta(1/\bar{I}_b^{pu} - 1) + 1} \Delta_b^I \\ &= \left(\frac{1}{\theta(1/\bar{I}_b^{pu} - 1) + 1} \frac{1}{1 - \bar{I}_b^{pu}} - \frac{\bar{I}_b^{pu}}{1 - \bar{I}_b^{pu}} \right) \Delta_b^I \\ &= \left(\frac{1}{\theta(1 - \bar{I}_b^{pu}) + \bar{I}_b^{pu}} - 1 \right) \frac{\bar{I}_b^{pu}}{1 - \bar{I}_b^{pu}} \Delta_b^I,\end{aligned}$$

where $\Delta_b^I = (\mathbf{I}_b^{pu} - \bar{I}_b^{pu} \mathbf{1}_N) / \bar{I}_b^{pu}$. It is straightforward to conclude that $\Delta^I(\theta)$ is monotonous on $\theta \in [0, 1]$. Moreover, letting $\theta = 1$ yields $\Delta^I(1) = \mathbf{0}$. Thus, $|\Delta^I(\theta)|$ is monotonically decreasing on $\theta \in [0, 1]$. \square

Corollary 1 *Considering a DC microgrid with the same conditions and control laws as in Theorem 1, the following control objectives can be achieved:*

- (a) Accurate current sharing is achieved when $\theta = 1$;
- (b) Accurate voltage consensus is achieved, when $\theta = 0$;
- (c) A voltage-current compromise is achieved when $\theta \in (0, 1)$.

Proof: See Appendix B. \square

3.4 Voltage deviation restriction

According to Theorem 1, the secondary control law (9) essentially manipulates VDR and CDR by the trade-off factor θ . In subsequence, the tuning rule of the trade-off factor is characterized subject to given admissible MVDR.

Proposition 1 *Consider a DC microgrid with the same conditions and control laws as in Theorem 1. For given admissible maximum voltage deviation ratio Γ_V , voltage deviation restriction can be achieved, i.e., $\Delta_{max}^V(\theta) \leq \Gamma_V, \forall \theta \in [0, \theta_d]$, where*

$$\theta_d = \begin{cases} 1, & \text{if } \|\Delta^V(1)\|_\infty < \Gamma_V \\ \frac{\Gamma_V}{\|\Psi\|_\infty - \Gamma_V(\mu - 1)}, & \text{if } \Gamma_V \in (0, \|\Delta^V(1)\|_\infty] \\ 0, & \text{if } \Gamma_V = 0. \end{cases}$$

Proof: See Appendix C. \square

So far Problem 1 has been addressed jointly by Theorem 1, Corollary 1, and Proposition 1.

4 Voltage balancing and compromised control of critical nodes

4.1 Critical node, ordinary node, and problem formulation

In DC microgrids, it is necessary to restrict voltage deviations of buses connecting to voltage-sensitive loads within admissible ranges to guarantee normal operations of the loads, but there are no rigorous requirements on voltage deviation of buses connecting to voltage-insensitive loads. Therefore, it is intuitive to classify the nodes in the DC microgrid as critical nodes and ordinary nodes, and set different control objectives for the two kinds of nodes respectively.

For a DC microgrid with N nodes, without loss of generality, suppose nodes $\{1, \dots, m\}$ are critical nodes, and nodes $\{m + 1, \dots, N\}$ are ordinary nodes. Then, let

$$\bar{\mathbf{Y}} = \mathbf{Y} + \mathbf{Y}_L = \begin{bmatrix} \bar{\mathbf{Y}}_{11} & \mathbf{Y}_{12} \\ \mathbf{Y}_{21} & \bar{\mathbf{Y}}_{22} \end{bmatrix}, \text{ where } \bar{\mathbf{Y}}_{11} \in \mathbb{R}^{m \times m}, \mathbf{Y}_{12} \in$$

$\mathbb{R}^{m \times (N-m)}, \mathbf{Y}_{21} \in \mathbb{R}^{(N-m) \times m}, \bar{\mathbf{Y}}_{22} \in \mathbb{R}^{(N-m) \times (N-m)}$. Hence, the steady state equation (6b) can be rewritten in partitioned matrix form,

$$\begin{bmatrix} \mathbf{I}_1 \\ \mathbf{I}_2 \end{bmatrix} = \begin{bmatrix} \bar{\mathbf{Y}}_{11} & \mathbf{Y}_{12} \\ \mathbf{Y}_{21} & \bar{\mathbf{Y}}_{22} \end{bmatrix} \begin{bmatrix} \mathbf{V}_1 \\ \mathbf{V}_2 \end{bmatrix}, \quad (20)$$

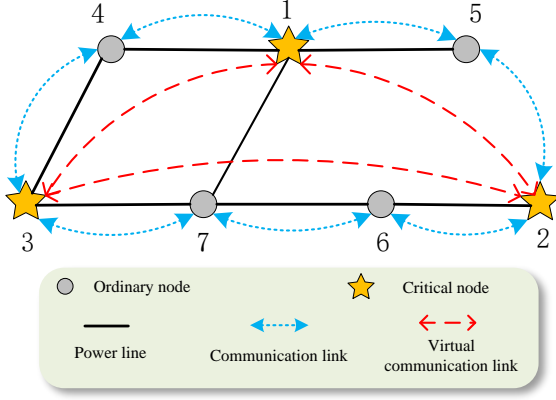


Fig. 3. Kron reduction for the communication network of a DC microgrid with 7 buses

where $\mathbf{I}_1, \mathbf{V}_1 \in \mathbb{R}^m$ denote the steady state currents and voltages of critical nodes, respectively; and $\mathbf{I}_2, \mathbf{V}_2 \in \mathbb{R}^{N-m}$ are similarly defined for ordinary nodes.

The second problem considered in this paper is formulated as follows.

Problem 2 Consider a DC microgrid described by (20) in steady state.

- For critical nodes, the control objective is to achieve voltage balancing and voltage deviation restriction, i.e., $\frac{1}{N} \mathbf{1}_m^T \mathbf{V}_1 = V_{rat}$, $\Delta_{max}^{V_1} \leq \Gamma_V$, where $\Delta_{max}^{V_1} = \|\Delta_1^V\|_\infty = \max_i \frac{|V_i - V_{rat}|}{V_{rat}}, \forall i \in \{1, \dots, m\}$, with Δ_1^V and $\Delta_{max}^{V_1}$ denoting the VDRs and the MVDR of the critical nodes respectively.
- For ordinary nodes, the control objective is to achieve accurate current sharing, i.e., $\frac{I_{m+1}}{I_{m+1}^*} = \dots = \frac{I_N}{I_N^*} = \alpha$ while the per-unit value α of output currents of DGs is tunable by control parameters.

4.2 Average voltage estimation for critical nodes

Kron reduction is often used in network reduction of electrical circuit, which effectively reduces the internal nodes of circuit topology (Caliskan and Tabuada, 2014; Dörfler et al., 2018). We shall apply Kron reduction to eliminate ordinary nodes of communication graph, thus realizing average voltage estimation of critical nodes. Based on this estimation, average voltage tracking of critical nodes will be achieved.

- For critical nodes ($i \in \{1, \dots, m\}$)

$$\dot{\tilde{V}}_i = \dot{V}_i + \sum_{j=1}^N a_{ij} (\tilde{V}_j - \tilde{V}_i) \quad (21)$$

where \tilde{V}_i is the estimation of average voltage among critical nodes observed by the i -th DG.

- For ordinary nodes ($k \in \{m+1, \dots, N\}$)

$$\tilde{V}_k = \frac{\sum_{j=1}^N a_{kj} \tilde{V}_j}{\sum_{j=1}^N a_{kj}}, \quad (22)$$

where a_{ij}, a_{kj} are the elements of the adjacency matrix \mathcal{A} of the communication graph $\mathcal{G}(\mathcal{A})$. As shown in Fig. 3, by utilizing Kron reduction, a generic communication network (blue dashed lines) is reduced as a virtual communication network (red dashed lines) among the critical nodes, aiming at an average voltage consensus of the critical nodes.

Proposition 2 Considering the DC microgrid (2) and (3) comprised of the critical nodes $\{1, \dots, m\}$ and the ordinary nodes $\{m+1, \dots, N\}$, in steady state, the estimation governed by (21) and (22) converges to the average voltage among the critical nodes, i.e.,

$$\lim_{t \rightarrow \infty} \tilde{V}_i = \frac{1}{m} \sum_{j=1}^m V_j, \quad \forall i \in \{1, \dots, N\}. \quad (23)$$

Proof: See Appendix D. \square

4.3 Compromised control for critical nodes

The control laws to simultaneously achieve both voltage-current compromise of critical nodes and accurate current sharing of ordinary nodes are proposed as follows.

- For critical nodes ($i \in \{1, \dots, m\}$)

$$u_i = V_{rat} - r_i I_i + \delta_i^I + \delta_i^V \quad (24a)$$

$$\delta_i^I = \sum_{j=1}^N a_{ij} (I_j^{pu} - I_i^{pu}) \quad (24b)$$

$$I_i^{pu} = \frac{I_i}{\theta I_i^* + (1-\theta) I_{b_i}} \quad (24c)$$

$$\delta_i^V = V_{rat} - \tilde{V}_i, \quad (24d)$$

where $\theta \in [0, 1]$ is the trade-off factor, and $\mathbf{I}_{b_1} = [I_{b_1}, \dots, I_{b_m}]^T \in \mathbb{R}^m$ with

$$\mathbf{I}_{b_1} = \omega V_{rat} \bar{\mathbf{Y}}_{22} | \bar{\mathbf{Y}} \mathbf{1}_m + \mathbf{Y}_{12} \bar{\mathbf{Y}}_{22}^{-1} \mathbf{I}_2^*,$$

where $\bar{\mathbf{Y}}_{22} | \bar{\mathbf{Y}} = \bar{\mathbf{Y}}_{11} - \mathbf{Y}_{12} \bar{\mathbf{Y}}_{22}^{-1} \mathbf{Y}_{21}$. $\omega > 0$ is utilized to adjust the output current of ordinary nodes.

- For ordinary nodes ($k \in \{m+1, \dots, N\}$)

$$u_k = V_{rat} - r_k I_k + \delta_k^I \quad (25a)$$

$$\delta_k^I = \sum_{j=1}^N a_{kj} (I_j^{pu} - I_k^{pu}) \quad (25b)$$

$$I_k^{pu} = \frac{I_k}{I_k^*}. \quad (25c)$$

For a given DC microgrid comprised of critical nodes and ordinary nodes, the degree of voltage-current compromise of critical nodes can be adjusted by tuning θ , which will be clarified in Corollary 2. Additionally, accurate current sharing of ordinary nodes can always be achieved independent of θ .

4.4 Analysis of steady state

Theorem 2 Consider the DC microgrid (2) and (3) comprised of the critical nodes $\{1, \dots, m\}$ and the ordinary nodes $\{m+1, \dots, N\}$. These two kinds of nodes are respectively governed by (24) and (25), and the average voltage among critical nodes is estimated by (21) and (22). Then, in steady state, the following statements hold:

- (a) Voltage balancing among critical nodes is achieved, i.e., $\tilde{V}_i = \frac{1}{m} \sum_{j=1}^m V_j = V_{rat}$.
- (b) For a given θ , the load current is shared proportionally among all DGs as

$$\begin{aligned} \frac{I_1}{I_{r_1}} = \dots = \frac{I_m}{I_{r_m}} = \frac{I_{m+1}}{I_{m+1}^*} = \dots = \frac{I_N}{I_N^*} \\ = \frac{1}{\mu\theta + \omega(1-\theta)}, \end{aligned} \quad (26)$$

where $\mu = \frac{1}{mV_{rat}} \mathbb{1}_m^T (\bar{\mathbf{Y}}_{22} | \bar{\mathbf{Y}})^{-1} (\mathbf{I}_1^* - \mathbf{Y}_{12} \bar{\mathbf{Y}}_{22}^{-1} \mathbf{I}_2^*)$. In addition, the output per-unit currents of the DGs at critical nodes are

$$\begin{aligned} \mathbf{I}_1^{pu} &= \text{diag}(\mathbf{I}_1^*)^{-1} \mathbf{I}_1 \\ &= \frac{\theta \mathbb{1}_m + (1-\theta) \text{diag}(\mathbf{I}_1^*)^{-1} \mathbf{I}_{b_1}}{\mu\theta + \omega(1-\theta)}. \end{aligned}$$

- (c) Function $|\Delta_1^V(\theta)|$ is monotonically increasing on $\theta \in [0, 1]$, and

$$\Delta_1^V(\theta) = \frac{\theta}{(\mu - \omega)\theta + \omega} \Psi_1, \quad (27)$$

where $\Psi_1 = \frac{1}{V_{rat}} (\bar{\mathbf{Y}}_{22} | \bar{\mathbf{Y}})^{-1} (\mathbf{I}_1^* - \mathbf{Y}_{12} \bar{\mathbf{Y}}_{22}^{-1} \mathbf{I}_2^*) -$

$\mu \mathbb{1}_m$. Particularly, for $\theta \in [0, 1]$, we have

$$\begin{cases} \min_{\theta} |\Delta_1^V(\theta)| = \Delta_1^V(0) = 0 \\ \max_{\theta} |\Delta_1^V(\theta)| = |\Delta_1^V(1)| = \frac{1}{\mu} |\Psi_1|. \end{cases} \quad (28)$$

- (d) Let $\Delta_1^I(\theta)$ denote the current deviation ratios of the critical nodes. Then, $|\Delta_1^I(\theta)|$ is monotonically decreasing on $\theta \in [0, 1]$, and

$$\Delta_1^I(\theta) = \frac{1 - \theta}{\theta (1/\bar{I}_{b_1}^{pu} - 1) + 1} \Delta_{b_1}^I,$$

where $\bar{I}_{b_1}^{pu} = \frac{1}{m} \mathbb{1}_m^T \mathbf{I}_{b_1}^{pu}$ and $\Delta_{b_1}^I = (\mathbf{I}_{b_1}^{pu} - \bar{I}_{b_1}^{pu} \mathbb{1}_m) / \bar{I}_{b_1}^{pu}$ with $\mathbf{I}_{b_1}^{pu} = \text{diag}(\mathbf{I}_1^*)^{-1} \mathbf{I}_{b_1}$. Particularly, for $\theta \in [0, 1]$, we have

$$\begin{cases} \min_{\theta} |\Delta_1^I(\theta)| = \Delta_1^I(1) = 0 \\ \max_{\theta} |\Delta_1^I(\theta)| = |\Delta_1^I(0)| = |\Delta_{b_1}^I|. \end{cases}$$

- (e) Bus voltage of ordinary nodes \mathbf{V}_2 is as follows.

$$\mathbf{V}_2 = \frac{1}{\theta(\mu - \omega) + \omega} \left(\Omega_2 - \frac{\omega}{\mu - \omega} \Omega_1 \right) + \frac{1}{\mu - \omega} \Omega_1,$$

where $\Omega_1 = -(\bar{\mathbf{Y}}_{11} | \bar{\mathbf{Y}})^{-1} \mathbf{Y}_{21} \bar{\mathbf{Y}}_{11}^{-1} (\mathbf{I}_1^* - \mathbf{I}_{b_1})$ and $\Omega_2 = (\bar{\mathbf{Y}}_{11} | \bar{\mathbf{Y}})^{-1} (\mathbf{I}_2^* - \mathbf{Y}_{21} \bar{\mathbf{Y}}_{11}^{-1} \mathbf{I}_{b_1})$. Each entry of \mathbf{V}_2 is a monotone function on $\theta \in [0, 1]$.

Proof: Part (a).

According to Proposition 2, it holds that $\tilde{V}_i = \frac{1}{m} \sum_{j=1}^m V_j$ in steady state. Considering $\delta_i^V = 0$ in (24d), we have $\tilde{V}_i = \frac{1}{m} \sum_{j=1}^m V_j = V_{rat}$.

Part (b).

Equation (20) can be rewritten as follows

$$\begin{cases} \mathbf{I}_1 = \bar{\mathbf{Y}}_{11} \mathbf{V}_1 + \mathbf{Y}_{12} \mathbf{V}_2, \\ \mathbf{I}_2 = \mathbf{Y}_{21} \mathbf{V}_1 + \bar{\mathbf{Y}}_{22} \mathbf{V}_2. \end{cases}$$

Then, the following identity holds

$$\mathbf{I}_1 = (\bar{\mathbf{Y}}_{11} - \mathbf{Y}_{12} \bar{\mathbf{Y}}_{22}^{-1} \mathbf{Y}_{21}) \mathbf{V}_1 + \mathbf{Y}_{12} \bar{\mathbf{Y}}_{22}^{-1} \mathbf{I}_2. \quad (29)$$

According to steady state analysis in Nasirian et al. (2015), it is straightforward to yield

$$\frac{I_1}{I_{r_1}} = \dots = \frac{I_m}{I_{r_m}} = \frac{I_{m+1}}{I_{m+1}^*} = \dots = \frac{I_N}{I_N^*}.$$

Additionally, letting $\mathbf{I}_1 = \alpha \mathbf{I}_{r_1} = \alpha(\theta \mathbf{I}_1^* + (1-\theta) \mathbf{I}_{b_1})$ and $\mathbf{I}_2 = \alpha \mathbf{I}_2^*$ and substituting them into (29) yields

$$\begin{aligned}
\Delta_1^V(\theta) &= \frac{1}{\theta\mu + \omega(1-\theta)} (\bar{\mathbf{Y}}_{22}|\bar{\mathbf{Y}})^{-1} \left(\frac{\theta}{V_{rat}} (\mathbf{I}_1^* - \mathbf{I}_{b_1}) + \omega \bar{\mathbf{Y}}_{22}|\bar{\mathbf{Y}} \mathbb{1}_m \right) - \mathbb{1}_m \\
&= \frac{\omega}{\theta(\mu - \omega) + \omega} \left(\mathbb{1}_m - \frac{1}{\mu - \omega} \left(\frac{1}{V_{rat}} (\bar{\mathbf{Y}}_{22}|\bar{\mathbf{Y}})^{-1} (\mathbf{I}_1^* - \mathbf{Y}_{12} \bar{\mathbf{Y}}_{22}^{-1} \mathbf{I}_2^*) - \omega \mathbb{1}_m \right) \right) \\
&\quad + \frac{1}{\mu - \omega} \left(\frac{1}{V_{rat}} (\bar{\mathbf{Y}}_{22}|\bar{\mathbf{Y}})^{-1} (\mathbf{I}_1^* - \mathbf{Y}_{12} \bar{\mathbf{Y}}_{22}^{-1} \mathbf{I}_2^*) - \omega \mathbb{1}_m \right) - \mathbb{1}_m \\
&= \frac{\theta}{\theta\mu + \omega - \theta\omega} \Psi_1.
\end{aligned} \tag{33}$$

$\alpha(\theta(\mathbf{I}_1^* - \mathbf{I}_{b_1}) + \mathbf{I}_{b_1}) = \bar{\mathbf{Y}}_{22}|\bar{\mathbf{Y}} \mathbf{V}_1 + \mathbf{Y}_{12} \bar{\mathbf{Y}}_{22}^{-1} \alpha \mathbf{I}_2^*$. In addition, voltage balancing for critical nodes implies $\mathbf{V}_1 = V_{rat}(\mathbb{1}_m + \Delta_1^V)$ with $\mathbb{1}_m^T \Delta_1^V = 0$. Consequently, we have

$$\begin{aligned}
\alpha (\bar{\mathbf{Y}}_{22}|\bar{\mathbf{Y}})^{-1} (\theta(\mathbf{I}_1^* - \mathbf{I}_{b_1}) + \omega V_{rat} \bar{\mathbf{Y}}_{22}|\bar{\mathbf{Y}} \mathbb{1}_m) \\
= V_{rat} (\mathbb{1}_m + \Delta_1^V).
\end{aligned} \tag{30}$$

Pre-multiplying both sides of (30) by $\mathbb{1}_m^T$ gives

$$\alpha = \frac{1}{\theta\mu + \omega(1-\theta)}. \tag{31}$$

Since $\omega > 0, \theta \in [0, 1]$ and $\mu > 0$, it is obvious that $\alpha > 0$.

Moreover, it can be further obtained that

$$\mathbf{I}_1 = \frac{1}{\mu\theta + \omega(1-\theta)} \mathbf{I}_r.$$

Substituting $\mathbf{I}_r = \theta \mathbf{I}_1^* + (1-\theta) \mathbf{I}_{b_1}$ into the above equation and considering $\mathbf{I}_1^{pu} = \text{diag}(\mathbf{I}_1^*)^{-1} \mathbf{I}_1$, we have

$$\mathbf{I}_1^{pu} = \frac{\theta}{\mu\theta + \omega(1-\theta)} \mathbb{1}_m + \frac{1-\theta}{\mu\theta + \omega(1-\theta)} \text{diag}(\mathbf{I}_1^*)^{-1} \mathbf{I}_{b_1}. \tag{32}$$

Part (c).

Substituting (31) in (30) and straightforward manipulation yields (33), i.e., (27) holds. Therefore, since $\alpha > 0$, it holds that $\frac{\theta}{\mu\theta + \omega - \theta\omega} \geq 0$. The function $|\Delta^V(\theta)|$ is monotonically increasing for $\theta \in [0, 1]$. Furthermore, it is straightforward to obtain (28).

Part (d).

The proof follows the same steps as that of part (ii) in Theorem 1, and thus is omitted.

Part (e).

According to (20), the output currents of DGs at ordinary nodes are expressed as

$$\mathbf{I}_2 = (\bar{\mathbf{Y}}_{22} - \mathbf{Y}_{21} \bar{\mathbf{Y}}_{11}^{-1} \mathbf{Y}_{12}) \mathbf{V}_2 + \mathbf{Y}_{21} \bar{\mathbf{Y}}_{11}^{-1} \mathbf{I}_1 \tag{34}$$

Considering, in steady state, $\mathbf{I}_2 = \alpha \mathbf{I}_2^*$ and $\mathbf{I}_1 =$

$\alpha(\theta \mathbf{I}_1^* + (1-\theta) \mathbf{I}_{b_1})$, we have

$$\alpha (\mathbf{I}_2^* - \mathbf{Y}_{21} \bar{\mathbf{Y}}_{11}^{-1} (\theta \mathbf{I}_1^* + (1-\theta) \mathbf{I}_{b_1})) = \bar{\mathbf{Y}}_{11}|\bar{\mathbf{Y}} \mathbf{V}_2$$

Then, substituting (31) into the above equation yields $\mathbf{V}_2 = \frac{1}{\theta\mu + \omega(1-\theta)} (\theta \Omega_1 + \Omega_2)$. Furthermore, it is derived that each entry of \mathbf{V}_2 is a monotone function for $\theta \in [0, 1]$, and \mathbf{V}_2 is expressed as

$$\mathbf{V}_2 = \frac{1}{\theta(\mu - \omega) + \omega} \left(\Omega_2 - \frac{\omega}{\mu - \omega} \Omega_1 \right) + \frac{1}{\mu - \omega} \Omega_1.$$

This completes the proof. \square

Remark 3 Theorem 2 reduces to Theorem 1 when $m = N$ and $\omega = 1$. This implies that Theorem 1 is a special case of Theorem 2 where all nodes are critical nodes. In other words, all nodes are equally important.

Corollary 2 Consider a DC microgrid with the same conditions as Theorem 2. The objectives listed in Corollary 1 for critical nodes can be achieved.

Proof. Similar to that of Corollary 1. \square

4.5 Voltage deviation restriction for critical nodes

The following proposition demonstrates the design of the trade-off factor to achieve voltage deviation restriction for the critical nodes.

Proposition 3 Consider a DC microgrid with the same conditions as those in Theorem 2. For given admissible maximum voltage deviation ratio Γ_V , voltage deviation restriction for the critical nodes is achieved when $\theta \in [0, \theta_d]$, where θ_d is designed as

$$\theta_d = \begin{cases} 1, & \text{if } \|\Delta_1^V(1)\|_\infty < \Gamma_V; \\ \frac{\omega \Gamma_V}{(\mu - \omega) (\|\Psi_1\|_\infty - \Gamma_V)}, & \text{if } \Gamma_V \in (0, \|\Delta_1^V(1)\|_\infty]; \\ 0, & \text{if } \Gamma_V = 0. \end{cases}$$

Proof. The proof follows the similar development as

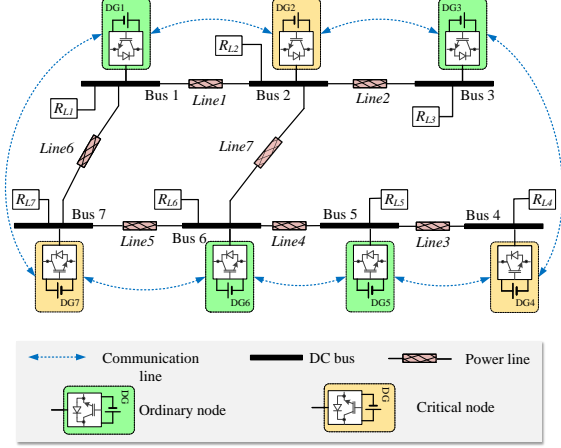


Fig. 4. DC microgrid with 7 buses

that of Proposition 1, and thus is omitted. \square

4.6 Output current adjustment for ordinary nodes

In addition to the trade-off factor θ , there is another tuning parameter ω in the control law (24). The following proposition gives the adjustable range of ω and shows the monotonicities of the output currents of DGs at the critical nodes and the ordinary nodes with respect to ω .

Proposition 4 Consider a DC microgrid with the same conditions as those in Theorem 2. For given $\theta \in [0, 1)$, the adjustable range of ω is

$$\omega \in \mathcal{W} = \left[\max_i \left\{ \frac{\zeta_i}{\nu_i} \right\}, +\infty \right), i \in \{1, \dots, m\}, \forall \nu_i > 0$$

where $\Xi_1 = [\zeta_i] = \frac{-\theta}{1-\theta} \mathbf{I}_1^* - \mathbf{Y}_{12} \bar{\mathbf{Y}}_{22}^{-1} \mathbf{I}_2^*$, $\Upsilon_1 = [\nu_i] = V_{rat} \bar{\mathbf{Y}}_{22} \bar{\mathbf{Y}} \mathbf{1}_m$. Moreover, the following statements hold.

- (a) The output per-unit currents of DGs at the ordinary nodes \mathbf{I}_2^{bu} are monotonically decreasing on $\omega \in \mathcal{W}$.
- (b) The sum of the output currents of DGs at the critical nodes $\mathbf{1}_m^T \mathbf{I}_1$ is monotonically increasing on $\omega \in \mathcal{W}$ if $\theta \mathbf{1}_m^T \mathbf{I}_1^* + (1-\theta) \mathbf{1}_m^T \mathbf{Y}_{12} \bar{\mathbf{Y}}_{22}^{-1} \mathbf{I}_2^* < 0$.

Proof: See Appendix E. \square

Therefore, Problem 2 is solved by Theorem 2, Corollary 2 and Proposition 3, 4.

5 Simulation examples

Consider a DC microgrid composed of 7 DGs, as shown in Fig. 4, where the interconnection communication network is depicted by blue dashed lines. Without loss of generality, let the weight of each communication link be $a_{ij} = 20$, where a greater a_{ij} is beneficial to faster

convergence to the steady state without changing the steady-state value (Lewis et al., 2014).

The rated voltage of the microgrid is set to $V_{rat} = 380V$. Let

$$\mathbf{I}^* = \text{diag}(30, 30, 20, 20, 40, 40, 40) \text{ A.}$$

The parameters of DGs and loads are

$$\mathbf{L}_t = \text{diag}(2, 2.2, 1.8, 2.5, 3, 2.6, 2.3) \text{ mH}$$

$$\mathbf{C}_t = \text{diag}(3, 2.5, 2.8, 2.5, 2.3, 3, 2.6) \text{ mF}$$

$$\mathbf{R}_L = \text{diag}(50, 20, 26, 35, 38, 23, 40) \Omega.$$

The parameters of power lines are: $R_{l_1} = 2\Omega$, $L_{l_1} = 20\mu\text{H}$; $R_{l_2} = 2.4\Omega$, $L_{l_2} = 25\mu\text{H}$; $R_{l_3} = 2\Omega$, $L_{l_3} = 20\mu\text{H}$; $R_{l_4} = 4\Omega$, $L_{l_4} = 35\mu\text{H}$; $R_{l_5} = 2\Omega$, $L_{l_5} = 20\mu\text{H}$; $R_{l_6} = 2\Omega$, $L_{l_6} = 20\mu\text{H}$; $R_{l_7} = 2\Omega$, $L_{l_7} = 20\mu\text{H}$.

The simulation example consists of two cases. In Case I, the comprised control law (9) is used for all nodes and voltage deviation restriction of all buses will be achieved. In Case II, voltage deviation restriction and voltage balancing of the critical nodes are considered with the controller governed by (21), (22), (24) and (25).

Case I: (Compromised control for all nodes)

In this case, an admissible MVDR is set to as $\Gamma_V = 3\%$. To illustrate the effectiveness of control law (9), we conduct a simulation in 3 phases, as shown in Fig. 5:

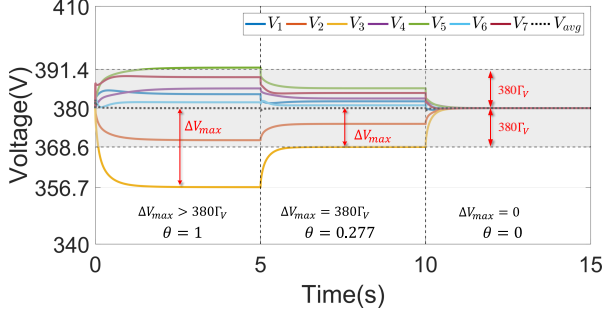
Phase 1: During $t \in [0, 5)s$, the trade-off factor θ is set to 1. Figure 5(b) shows that accurate current sharing is achieved. Meanwhile, it can be seen from Fig. 5(a) that $\Delta V_{max} = 380 - V_3 = 23.3V > 380\Gamma_V$ and $\Delta V_{max}^V(1) = 0.061 > \Gamma_V$. Thus, θ should be adjusted to meet the requirement of admissible MVDR.

Phase 2: During $t \in [5, 10)s$, the trade-off factor θ is set to 0.277. In fact, according to Theorem 1 and Proposition 1, $\Delta V_{max}^V(\theta) \in [0, 0.03]$ and $\Delta V_{max}^I(\theta) \in [0.358, 0.671]$, $\forall \theta \in [0, 0.277]$. It is shown in Fig. 5(a) that in steady state, ΔV_{max}^V is successfully restricted to $380\Gamma_V$, i.e., $\Delta V_{max}^V(0.277) = \Gamma_V$. This is achieved by sacrificing the degree of current sharing of all nodes, which is shown in Fig. 5(b).

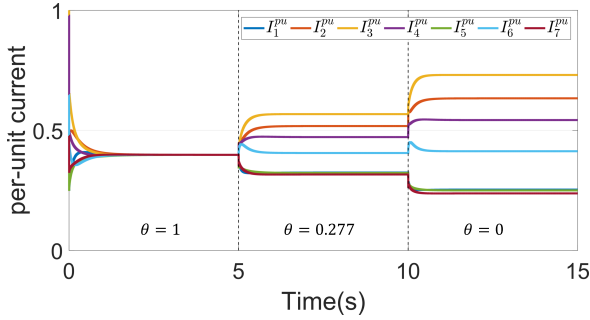
Phase 3: During $t \in (10, 15)s$, we further let $\theta = 0$ to reach bus voltage consensus, which is shown by Fig. 5(a). In this case, the current sharing performance is no longer considered.

From Case I, one can conclude that a compromise between voltage consensus and current sharing can be achieved using the proposed control law (9), and the degree of compromise can be adjusted by tuning the trade-off factor θ .

Case II: (Compromised control for critical nodes)



(a) Bus voltages



(b) Per-unit currents

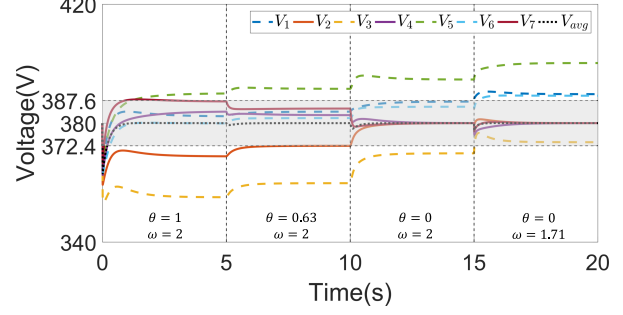
Fig. 5. Simulation results of Case I. The shaded area corresponds to the admissible voltage range for all nodes.

In this case, let nodes $\{2, 4, 7\}$ be the critical nodes, and the rest ones be ordinary nodes. For critical nodes, the objective is to restrict the voltage deviation within $[0, \Gamma_V]$, where $\Gamma_V = 2\%$, meanwhile maintaining the current sharing performance of ordinary nodes. To illustrate the effectiveness of control laws (21), (22), (24) and (25), we conduct the simulation in 4 phases.

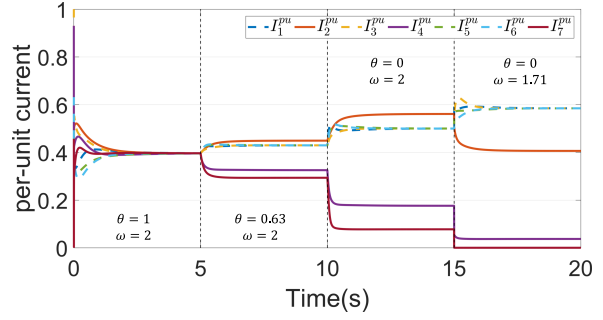
Phase 1: During $t \in [0, 5]s$, let $\theta = 1, \omega = 2$ in controller (24). In steady state, Fig. 6(b) shows current sharing for all nodes is achieved, while Fig. 6(a) shows the voltage deviation of node 7 is beyond the admissible range (shaded area).

Phase 2: During $t \in [5, 10]s$, we set $\theta = 0.63$ and $\omega = 2$. In fact, according to Theorem 2 and Proposition 3, the MVDR of critical nodes can be restricted within $[0, 0.02]$ by setting $\theta \in [0, 0.63]$ when $\omega = 2$, which is shown in Fig. 6(a). At the same time, the current sharing performance of critical nodes is degraded, which shows a compromise between voltage consensus and current sharing of critical nodes. It is noted from Fig. 6(b) that the current sharing of ordinary nodes is still maintained.

Phase 3: During $t \in [10, 15]s$, we set $\theta = 0$ and $\omega = 2$ to achieve voltage consensus of critical nodes, which can be shown in Fig. 6(a). In this case, the critical nodes have the worst current sharing performance (see Fig. 6(b)).



(a) Bus voltages



(b) Per-unit currents

Fig. 6. Simulation results of Case II. The shaded area corresponds to the admissible voltage range for critical nodes.

At the same time, the current sharing is still achieved for ordinary nodes.

Phase 4: During $t \in [15, 20]s$, by tuning ω from 2 to 1.71, the output currents of ordinary nodes increase. Meanwhile, the output currents of critical nodes decrease accordingly. Also note that when $\omega = 1.71$, $I_7^{pu} = 0$, the per-unit currents of ordinary nodes reach the admissible maximum $I_i^{pu} = 0.585, i = \{1, 3, 5, 6\}$ (see Fig. 6(b)). In this phase, since $\theta = 0$, the voltage consensus for critical nodes still holds (see Fig. 6(a)).

Moreover, we can see that the average voltage of critical nodes can always be regulated to the rated value of 380V (see Fig. 6(a)), and current sharing for ordinary nodes can also be achieved (see Fig. 6(b)), both independent of the choices of θ and ω .

Case III: (Plug-and-play setting of ordinary nodes)

In this case, the settings of critical nodes and ordinary nodes are the same as in Case II. Let $\theta = 0$ and $\omega = 2$. This setting corresponds to accurate voltage consensus of critical nodes and accurate current sharing of ordinary nodes. To illustrate the performance of the proposed control laws against the plug-and-play of DGs, we conduct the simulation in three phases.

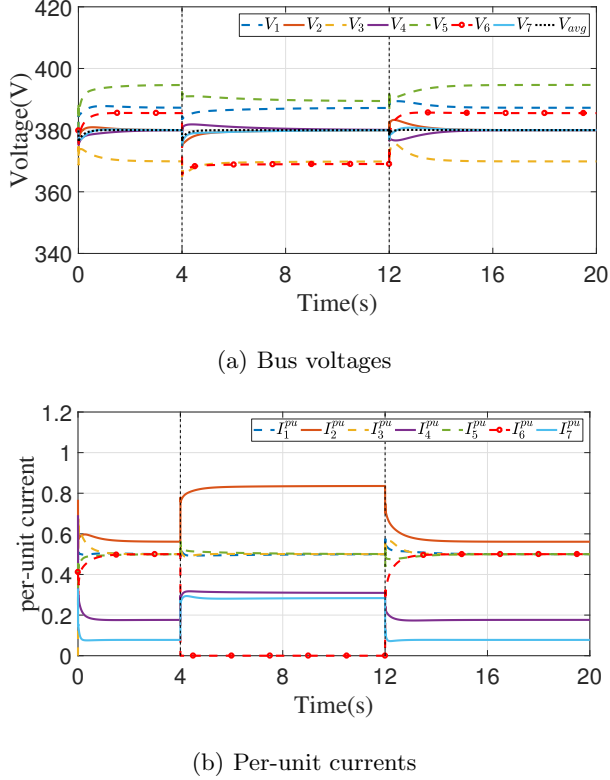


Fig. 7. Simulation results of Case III. At $t = 4s$, DG 6 is unplugged, and then at $t = 12s$, DG 6 is again plugged back into the microgrid.

Phase 1: During $t \in [0, 4)s$, all nodes are normally operated. Figure 7(a) shows that all critical node voltages are regulated to 380V, i.e., accurate voltage consensus is achieved. At the same time, currents are accurately shared among all ordinary nodes (i.e., 1, 3, 5, 6) (see Fig. 7(b)).

Phase 2: During $t \in [4, 12)s$, the DG of node 6 is plugged out from the DC microgrid. Then the output current of DG 6 becomes zero immediately at $t = 4s$ (see Fig. 7(b)), and meanwhile, the bus voltage of node 6 is dropped from 385.5V to 369V (see Fig. 7(a)). However, voltage consensus of critical nodes and accurate current sharing of the rest ordinary nodes can still be achieved at steady state.

Phase 3: During $t \in [12, 20)s$, the DG of node 6 is plugged back into the DC microgrid. It can be observed from Fig. 7 that the behavior of bus voltage and per-unit current of all nodes is restored to the state before unplugging of DG 6.

6 Conclusion

This paper proposes a voltage-current compromised control scheme for multi-bus DC microgrids. By introducing two performance indices, i.e., voltage deviation ratio

and current deviation ratio, we formulated three objectives of accurate current sharing, accurate voltage consensus and voltage-current compromise in a unified manner, and figured out a necessary and sufficient condition for the conflict between accurate current sharing and accurate voltage consensus. For a class of DC microgrids with equally important nodes, we proposed a distributed compromised control law such that the maximum bus voltage deviation can be restricted as required, and the degree of compromise between voltage deviation and current sharing can be continuously adjusted by tuning only one trade-off parameter. It is worth noting that the proposed algorithm can extend various existing current sharing control methods to a compromised objective. Based on this control law, we further proposed a distributed compromised control law for a class of DC microgrids with both critical nodes and ordinary nodes. The bus voltage deviation of all critical nodes can be arbitrarily restricted without sacrificing accurate current sharing of those ordinary nodes. This control algorithm works also under plug-and-play settings. Extensive simulation examples illustrate the efficacy of the proposed algorithms.

Appendix

A Proof of Lemma 1

Based on the dynamic model of the DC microgrid (1), (2) and (3), the steady-state model of the DC microgrid can be derived as (6). The left-hand side of (4) can be deduced as

$$(\mathbf{Y} + \mathbf{Y}_L)^{-1} \mathbf{Y}_L \mathbf{1}_N = \left(\mathbf{E} - (\mathbf{Y} + \mathbf{Y}_L)^{-1} \mathbf{Y} \right) \mathbf{1}_N,$$

where \mathbf{E} denotes the identity matrix with compatible dimensions. Due to $\mathbf{Y} \mathbf{1}_N = \mathbf{0}$, (4) can be derived.

B Proof of Corollary 1

(a) When $\theta = 1$, it holds that $\mathbf{I}_r = \mathbf{I}^*$. Hence, in steady state, accurate current sharing is achieved.

(b) When $\theta = 0$, one can conclude $\mathbf{I}_r = \mathbf{I}_b$. Consequently, it implies, in steady state, that \mathbf{I} is proportional to $\mathbf{Y}_L \mathbf{1}_N$. According to Fact 1, accurate voltage consensus is achieved.

(c) When $\theta \in (0, 1)$, due to the monotonicity of $|\Delta^V(\theta)|$ and $|\Delta^I(\theta)|$, it holds that $|\Delta^V(1)| \geq |\Delta^V(\theta)| \geq |\Delta^V(0)|$ and $|\Delta^I(1)| \leq |\Delta^I(\theta)| \leq |\Delta^I(0)|$. Hence, we say that a compromise between accurate current sharing and voltage consensus is achieved.

C Proof of Proposition 1

According to (12), it is trivial to obtain that $\theta_d = 1$ (or $\theta_d = 0$) if $\|\Delta^V(1)\|_\infty < \Gamma_V$ (or $\Gamma_V = 0$). Then, according to (11) and considering $\mu > 0$, for given Γ_V , if $\Gamma_V \in (0, \|\Delta^V(1)\|_\infty]$, it holds that

$$\Gamma_V = \max_{\theta} \|\Delta^V(\theta)\|_\infty = \frac{\theta_d}{(\mu - 1)\theta_d + 1} \|\Psi\|_\infty,$$

which is further simplified to yield

$$\theta_d = \frac{\Gamma_V}{\|\Psi\|_\infty - \Gamma_V(\mu - 1)}.$$

D Proof of Proposition 2

One can rewrite (21) and (22) in compact form as follows,

$$\begin{bmatrix} \dot{\tilde{V}}_1 \\ 0 \end{bmatrix} = \begin{bmatrix} \dot{V}_1 \\ 0 \end{bmatrix} - \begin{bmatrix} \mathcal{L}_{11} & \mathcal{L}_{12} \\ \mathcal{L}_{21} & \mathcal{L}_{22} \end{bmatrix} \begin{bmatrix} \tilde{V}_1 \\ \tilde{V}_2 \end{bmatrix}. \quad (\text{D.1})$$

Then, it holds that $\dot{\tilde{V}}_1 = \dot{V}_1 - (\mathcal{L}_{11} - \mathcal{L}_{12}\mathcal{L}_{22}^{-1}\mathcal{L}_{21})\tilde{V}_1$, which is further simplified as

$$\dot{\tilde{V}}_1 = \dot{V}_1 - \mathcal{L}_{22}|\mathcal{L}\tilde{V}_1,$$

where $\mathcal{L}_{22}|\mathcal{L}$ is the Schur complement of Laplacian \mathcal{L} . Since the graph associated with \mathcal{L} is undirected and connected, according to Dörfler and Bullo (2013), $\mathcal{L}_{22}|\mathcal{L}$ is a symmetric Laplacian, and the graph associated with $\mathcal{L}_{22}|\mathcal{L}$ is undirected and connected. Hence, according to Kia et al. (2019), we have $\lim_{t \rightarrow \infty} \tilde{V}_i = \frac{1}{m} \sum_{j=1}^m V_j$, $i \in \{1, \dots, N\}$.

E Proof of Proposition 4

The range of ω is determined by the admissible range of the output currents of DGs. According to the statement (a) of Theorem 2, in steady state, the output per-unit currents of DGs at critical nodes are shown as

$$\begin{aligned} \mathbf{I}_2^{pu} &= \frac{1}{\mu\theta + \omega(1-\theta)} \\ \mathbf{I}_1^{pu} &= \text{diag}(\mathbf{I}_1^*)^{-1} \mathbf{I}_1 \\ &= \frac{\theta}{\mu\theta + \omega(1-\theta)} \mathbb{1}_m + \frac{1-\theta}{\mu\theta + \omega(1-\theta)} \text{diag}(\mathbf{I}_1^*)^{-1} \mathbf{I}_{b_1}. \end{aligned}$$

Since $\mathbf{I}_i^{pu} = \frac{I_i}{I_i^*} \geq 0, \forall i \in \{1, \dots, N\}$, and $\mathbf{I}_{b_1} = \omega V_{rat} \bar{\mathbf{Y}}_{22} |\bar{\mathbf{Y}} \mathbb{1}_m + \mathbf{Y}_{12} \bar{\mathbf{Y}}_{22}^{-1} \mathbf{I}_2^*$, we have

$$(1-\theta) (\omega V_{rat} \bar{\mathbf{Y}}_{22} |\bar{\mathbf{Y}} \mathbb{1}_m + \mathbf{Y}_{12} \bar{\mathbf{Y}}_{22}^{-1} \mathbf{I}_2^*) \geq -\theta \mathbf{I}_1^*.$$

Further considering $\bar{\mathbf{Y}}_{22} |\bar{\mathbf{Y}} \mathbb{1}_m \geq 0$ and $\bar{\mathbf{Y}}_{22} |\bar{\mathbf{Y}} \mathbb{1}_m \neq 0$ yields

$$\omega \in \mathcal{W} = \left[\max_i \left\{ \frac{\zeta_i}{\nu_i} \right\}, +\infty \right), i \in \{1, \dots, m\}, \forall \nu_i \neq 0.$$

where $\Xi_1 = [\zeta_i] = \frac{-\theta}{1-\theta} \mathbf{I}_1^* - \mathbf{Y}_{12} \bar{\mathbf{Y}}_{22}^{-1} \mathbf{I}_2^*$, $\Upsilon_1 = [\nu_i] = V_{rat} \bar{\mathbf{Y}}_{22} |\bar{\mathbf{Y}} \mathbb{1}_m$.

(a) Since $\mathbf{I}_2^{pu} = \frac{1}{\mu\theta + \omega(1-\theta)}$, it is straightforward to show the monotonic decreasing property of \mathbf{I}_2^{pu} on $\omega \in \mathcal{W}$.

(b)

$$\begin{aligned} \mathbb{1}_m^T \mathbf{I}_1 &= \frac{\theta}{\mu\theta + \omega(1-\theta)} \mathbb{1}_m^T \mathbf{I}_1^* + \frac{1-\theta}{\mu\theta + \omega(1-\theta)} \mathbb{1}_m^T \mathbf{I}_{b_1} \\ &= \eta_1 + \eta_2, \end{aligned}$$

where

$$\begin{cases} \eta_1 = \frac{(1-\theta) \omega V_{rat} \mathbb{1}_m^T \bar{\mathbf{Y}}_{22} |\bar{\mathbf{Y}} \mathbb{1}_m}{\mu\theta + \omega(1-\theta)} \\ \eta_2 = \frac{\theta \mathbb{1}_m^T \mathbf{I}_1^* + (1-\theta) \mathbb{1}_m^T \mathbf{Y}_{12} \bar{\mathbf{Y}}_{22}^{-1} \mathbf{I}_2^*}{\mu\theta + \omega(1-\theta)}. \end{cases}$$

Since $\theta \in [0, 1), \mu > 0$ and $\mathbb{1}_m^T \bar{\mathbf{Y}}_{22} |\bar{\mathbf{Y}} \mathbb{1}_m > 0$, η_1 is monotonically increasing on $\omega \in \mathcal{W}$. Moreover, since $\mathbb{1}_m^T \mathbf{Y}_{12} \bar{\mathbf{Y}}_{22}^{-1} \mathbf{I}_2^* < 0$, η_2 is monotonically increasing on $\omega \in \mathcal{W}$ if $\theta \mathbb{1}_m^T \mathbf{I}_1^* + (1-\theta) \mathbb{1}_m^T \mathbf{Y}_{12} \bar{\mathbf{Y}}_{22}^{-1} \mathbf{I}_2^* < 0$. Thus, the monotonic increasing property of $\mathbb{1}_m^T \mathbf{I}_1$ is established.

References

- Bai, H., Zhang, H., Cai, H., Schiffer, J., 2022. Voltage regulation and current sharing for multi-bus DC microgrids: a compromised design approach. *Automatica* 142, 110340.
- Caliskan, S.Y., Tabuada, P., 2014. Towards kron reduction of generalized electrical networks. *Automatica* 50, 2586–2590.
- Che, L., Shahidepour, M., 2014. DC microgrids: economic operation and enhancement of resilience by hierarchical control. *IEEE Transactions on Smart Grid* 5, 2517–2526.
- Cucuzzella, M., Trip, S., De Persis, C., Cheng, X., Ferrara, A., van der Schaft, A., 2018. A robust consensus algorithm for current sharing and voltage regulation in DC microgrids. *IEEE Transactions on Control Systems Technology* 27, 1583–1595.
- De Persis, C., Weitenberg, E.R., Dörfler, F., 2018. A power consensus algorithm for DC microgrids. *Automatica* 89, 364–375.
- Ding, L., Han, Q., Wang, L., Sindi, E., 2018. Distributed cooperative optimal control of DC microgrids with communication delays. *IEEE Transactions on Industrial Informatics* 14(9), 3924–3935.

- Dörfler, F., Bullo, F., 2013. Kron reduction of graphs with applications to electrical networks. *IEEE Transactions on Circuits and Systems I: Regular Papers* 60(1), 150–163.
- Dörfler, F., Simpson-Porco, J.W., Bullo, F., 2018. Electrical networks and algebraic graph theory: Models, properties, and applications. *Proceedings of the IEEE* 106, 977–1005.
- Dragičević, T., Lu, X., Vasquez, J.C., Guerrero, J.M., 2015. DC microgrids - Part I: A review of control strategies and stabilization techniques. *IEEE Transactions on Power Electronics* 31, 4876–4891.
- Elsayed, A.T., Mohamed, A.A., Mohammed, O.A., 2015. DC microgrids and distribution systems: An overview. *Electric Power Systems Research* 119, 407–417.
- Han, R., Wang, H., Jin, Z., Meng, L., Guerrero, J.M., 2019. Compromised controller design for current sharing and voltage regulation in DC microgrid. *IEEE Transactions on Power Electronics* 34(8), 8045–8061.
- Justo, J.J., Mwasilu, F., Lee, J., Jung, J.W., 2013. AC microgrids versus DC microgrids with distributed energy resources: A review. *Renewable and Sustainable Energy Reviews* 24, 387–405.
- Kia, S.S., Van Scoy, B., Cortes, J., Freeman, R.A., Lynch, K.M., Martinez, S., 2019. Tutorial on dynamic average consensus: the problem, its applications, and the algorithms. *IEEE Control Systems Magazine* 39, 40–72.
- Kundur, P., 1994. *Power System Stability and Control*. McGraw-Hill, New York.
- Lewis, F.L., Zhang, H., Hengster-Movric, K., Das, A., 2014. *Cooperative Control of Multi-Agent Systems: Optimal and Adaptive Design Approaches*. Springer, London.
- Liu, X., Wang, Y., Liu, Z., Huang, Y., 2023. On the stability of distributed secondary control for DC microgrids with grid-forming and grid-feeding converters. *Automatica* 155, 111164.
- Liu, Z., Su, M., Sun, Y., Han, H., Hou, X., Guerrero, J.M., 2018. Stability analysis of DC microgrids with constant power load under distributed control methods. *Automatica* 90, 62–72.
- Lund, H., 2007. Renewable energy strategies for sustainable development. *Energy* 32, 912–919.
- Nahata, P., Soloperto, R., Tucci, M., Martinelli, A., Ferrari-Trecate, G., 2020. A passivity-based approach to voltage stabilization in DC microgrids with zip loads. *Automatica* 113, 108770.
- Nahata, P., Turan, M.S., Ferrari-Trecate, G., 2022. Consensus-based current sharing and voltage balancing in DC microgrids with exponential loads. *IEEE Transactions on Control Systems Technology* 30, 1668–1680.
- Nasirian, V., Moayedi, S., Davoudi, A., Lewis, F.L., 2015. Distributed cooperative control of DC microgrids. *IEEE Transactions on Power Electronics* 30(4), 2288–2303.
- Prabhakaran, P., Goyal, Y., Agarwal, V., 2018. Novel nonlinear droop control techniques to overcome the load sharing and voltage regulation issues in DC microgrid. *IEEE Transactions on Power Electronics* 33(5), 4477–4487.
- Pratt, A., Kumar, P., Aldridge, T.V., 2007. Evaluation of 400v DC distribution in telco and data centers to improve energy efficiency, in: *Proc. of 29th International Telecommunications Energy Conference*, pp. 32–39. doi:10.1109/INTLEC.2007.4448733.
- Schiffer, J., Zonetti, D., Ortega, R., Stankovic, A.M., Sezi, T., Raisch, J., 2016. A survey on modeling of microgrids: From fundamental physics to phasors and voltage sources. *Automatica* 74, 135–150.
- Shafiee, Q., Dragičević, T., Vasquez, J.C., Guerrero, J.M., 2014. Hierarchical control for multiple DC-microgrids clusters. *IEEE Transactions on Energy Conversion* 29, 922–933.
- Trip, S., Cucuzzella, M., Cheng, X., Scherpen, J., 2019. Distributed averaging control for voltage regulation and current sharing in DC microgrids. *IEEE Control Systems Letters* 3, 174–179.
- Tucci, M., Meng, L., Guerrero, J.M., Trecate, G.F., 2018. Stable current sharing and voltage balancing in DC microgrids: A consensus-based secondary control layer. *Automatica* 95, 1–13.
- Zhao, J., Dörfler, F., 2015. Distributed control and optimization in DC microgrids. *Automatica* 61, 18–26.